Spectroscopic characterization of Ti-doped α-$ZnAl_2S_4$ spinel-type single crystals

2010 J. Phys.: Condens. Matter 22 055903

(http://iopscience.iop.org/0953-8984/22/5/055903)

J. Phys.: Condens. Matter **22** (2010) 055903 (6pp) doi:10.1088/0953-8984/22/5/055903

Spectroscopic characterization of Ti-doped α-$ZnAl_2S_4$ spinel-type single crystals

Sergiu Anghel[1,2], Georges Boulon[2], Alain Brenier[2], Emery Fortin[3], Sophia Klokishner[1], Dmitrii Koshchug[4], Leonid Kulyuk[1] and Konstantin Sushkevich[5]

[1] Institute of Applied Physics, Academiei Street 5, Chisinau MD-2028, Republic of Moldova
[2] Physical Chemistry of Luminescent Materials, Claude Bernard Lyon 1 University, UMR 5620 CNRS, Bâtiment Alfred Kastler, 10 rue Ampere, La Doua, F-69622 Villeurbanne, France
[3] Department of Physics, University of Ottawa, ON, K1N 6N5, Canada
[4] Geological Faculty, Moscow State University, Vorobievy Gory, Moscow 119899, Russia
[5] Department of Physics, Moldova State University, Alexei Mateevici Street 60, Chisinau MD-2009, Republic of Moldova

E-mail: anggell@gmail.com

Received 28 August 2009, in final form 20 December 2009
Published 19 January 2010
Online at stacks.iop.org/JPhysCM/22/055903

Abstract
The spectroscopic characteristics of the α-$ZnAl_2S_4$ wide bandgap semiconductor doped with Ti ions are investigated. It is shown, that the $ZnAl_2S_4$:Ti spinel-type crystals exhibit luminescence in the IR spectral range 0.8–1.4 μm. The observed spectroscopic characteristics are assigned to the emission bands arising from the ligand -Ti^{4+} charge transfer for octahedral sites of titanium that is in agreement with the experimental evidence for the absence of the EPR signal from Ti ions. A qualitative explanation of the experimental data is given.

(Some figures in this article are in colour only in the electronic version)

1. Introduction

Recently, there has been considerable interest in titanium-doped crystals as the active media for solid-state lasers. Besides the well-known Ti–sapphire (Al_2O_3:Ti) [1] there are several crystalline hosts where titanium ions manifest broad band luminescence in the near-IR and visible regions [2, 3] (and references therein). The spectroscopic properties of the Ti impurity in a spinel host crystal $MgAl_2O_4$ have been investigated in [4, 5] and blue emission with strong intensity was detected. Meanwhile, the interpretation of the spectroscopic properties of different oxides doped by titanium is not straightforward. Difficulties connected with the simultaneous presence in the host of Ti^{3+} and Ti^{4+} ions are met. In [6] it was revealed that the absorption spectrum of Ti^{3+}:Al_2O_3 crystals consists of the main blue-green absorption band and a weak infrared band. This infrared absorption decreases in intensity on annealing in a reducing atmosphere. Combined optical and EPR studies allowed the assumption that the center associated with the red band is a cluster involving Ti^{3+} and Ti^{4+} with a neighboring, charge compensating Al^{3+} vacancy. A similar problem to that observed in Ti^{3+}:Al_2O_3 has been reported for Ti^{3+}:$YAlO_3$, wherein a broad absorption is observed around 950 nm in addition to the normal visible absorption bands at 434 and 492 nm [7]. Two types of Ti^{4+} in Al_2O_3 (locally and nonlocally charge compensated) have been identified optically in [8]. The lifetimes of the charge-transfer emission as a function of temperature were well explained by a three-level scheme with a lower triplet excited state and a higher singlet excited state. The presence of Ti^{4+} occupying the Al^{3+} site in the spinel host was confirmed in [9]. As in [6–8] the mechanism proposed in [9] is based on the assumption of a charge-transfer excitation from O^{2-} ($2p\sigma$) into the empty (3d) orbital of Ti^{4+}, resulting in Ti^{3+} in the electronic excited state with a subsequent emission of a photon from this titanium 3d state stabilized by the interaction with lattice vibrations.

To obtain room-temperature IR sources of radiation the spectral properties of titanium-doped chalcogenides have also been intensively studied by many authors along with titanium-doped oxide compounds. In earlier publications absorption, photoconductivity and Hall measurements are reported on CdS [10–13] and CdSe [12, 14, 15]. In particular, the strong Ti^{2+} absorption bands determine the energies of the two

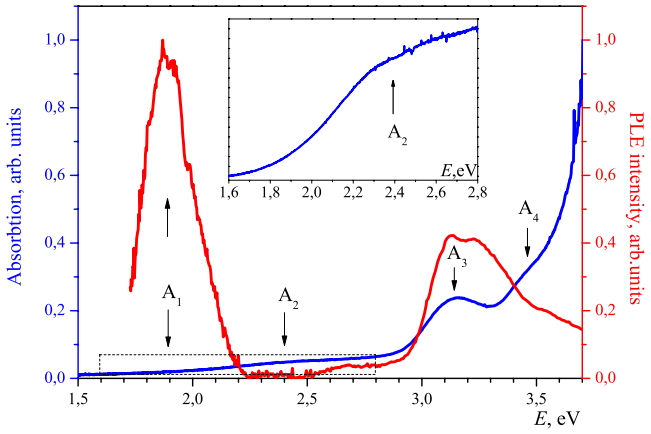

Figure 1. Absorption and PLE spectra of the α-$ZnAl_2S_4$:Ti single crystal.

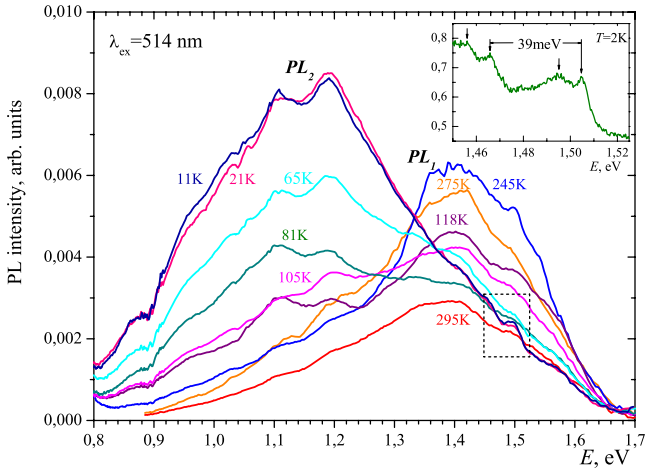

Figure 2. Emission spectra under 'green' excitation at different temperatures.

prominent transitions from $^3A_2(^3F)$ to $^3T_1(^3F)$ and $^3T_1(^3P)$ levels. A very weak absorption is also detected in both materials with maxima at about 3100 cm^{-1} in CdSe [14] and 3320 cm^{-1} in CdS [11]. This absorption has been assigned to the transition $^3A_2(^3F)$–$^3T_2(^3F)$ which is forbidden in T_d symmetry. An EPR investigation of the hyperfine interactions with ligand nuclei of the Ti^{2+} center in single crystals of hexagonal CdS and CdSe on sites with trigonal C_{3v} symmetry has been undertaken in [16, 17]. The experimental data obtained in [17] show that under irradiation of CdS:Ti^{2+} with light in the spectral region 400–800 nm no change of the EPR spectra could be observed. Irradiation with light of longer wavelengths results in a strong quenching and a line broadening of the EPR signal. The maximum quenching of the EPR spectrum was found to correspond to the maximum of the photoconductivity. The observed effect was explained by the depopulation of the $^3A_2$ term through the transitions to the excited levels that are in the conduction band of CdS. In [18] by EPR, the ground states of Ti^{2+} and Ti^{3+} were detected, indicating a substitutional incorporation of Ti ions into Cd sites in CdS, CdSe and Cd(S, Se) crystals. For the first time [18], the Jahn–Teller ion Ti^{3+} was observed by its $^2T_2 \rightarrow {}^2E$ transition in photoluminescence. Optical and paramagnetic properties of titanium centers in ZnS were examined in [19]. In this paper it was shown that the Ti^{2+} ion on a cubic site presents an isotropic EPR signal with $g = 1.928$ observable up to 80 K. Signals of Ti^{2+} ions on axial sites were detected in the same temperature range. In [19] it was also demonstrated that in emission the Ti^{2+} ion exhibits the $^3T_2(^3F) \rightarrow {}^3A_2(^3F)$ transition, structured by no-phonon lines of centers in various environments. The prominent line at 3613 cm^{-1} in the emission spectrum was assigned to the center with T_d symmetry, while the lines at 3636, 3634 and 3632 cm^{-1} were assumed to originate from the impurity centers in various trigonally distorted environments, as corroborated by the EPR data.

Thus, the titanium-doped systems demonstrate interesting peculiarities of the spectroscopic properties due to the possibility to embed Ti ions with different oxidation degrees into the host crystal. In some cases the simultaneous presence of impurity Ti^{2+} and Ti^{3+} ions can be observed [19]. However, all cited papers deal with titanium-doped chalcogenides or oxides. The present paper for the first time addresses the case of titanium-doped α-$ZnAl_2S_4$ spinel crystals wherein the Ti ions are in octahedral sulfur surroundings. We report extensive experimental characterization of the α-$ZnAl_2S_4$ including electron spin resonance and optical measurements. A qualitative explanation of the obtained experimental results is given.

2. Experimental results

Bulk stoichiometric α-$ZnAl_2S_4$:Ti crystals with impurity concentrations 0.1–0.5 at.% were grown by a closed tube vapor method with halogen as a transport agent [20]. The samples represented optically homogeneous octahedra with volumes up to 30 mm^3 and (111)-oriented mirrorlike faces which were used directly for photoluminescence experiments. For optical absorption and luminescence measurements some crystals were cut and polished in order to obtain flat parallel faces.

At temperatures $T = 10$–300 K the studies of the steady-state and time-resolved photoluminescence (PL) spectra, as well as of the PL excitation (PLE) and absorption spectra, were performed in the spectral range 0.4–1.5 μm using a liquid-nitrogen-cooled Ge detector or photomultiplier. The EPR studies of the samples were carried out as well.

At room temperature the optical absorption spectrum (figure 1) consists, at least, of three broad bands centered at $E_{A4} = 3.4$ eV, $E_{A3} = 3.1$ eV and $E_{A2} = 2.4$ eV, which can be attributed to the Ti impurity. The spectral edge observed at 3.6 eV corresponds to the host crystal intrinsic absorption [21, 22]. In order to provide the selective excitation of the impurity, the steady-state PL spectra were measured using, as excitation sources, the Ar^+ laser operating at $\lambda_{exG} = 514$ nm ('green' excitation, $E_{exG} = 2.41$ eV $\approx E_{A2}$) and He-Ne ('red' excitation, $\lambda_{exR} = 633$ nm) laser.

Under the 'green' excitation, the steady-state PL spectra of $ZnAl_2S_4$:Ti crystals consist of two broad bands centered at $E_{PL1} = 1.41$ eV and $E_{PL2} = 1.19$ eV (figure 2). The

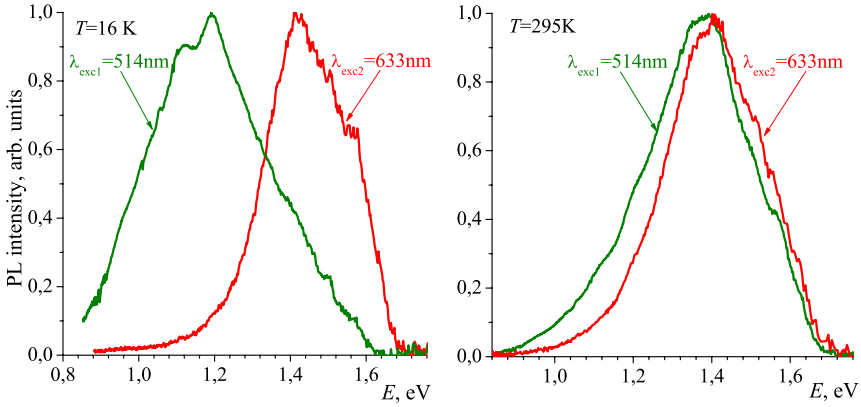

Figure 3. PL spectra under 'green' and 'red' excitations at low and room temperatures.

second component E_{PL2} dominates in the spectrum at low temperatures ($T < 80$ K). With a temperature rise the redistribution of the intensities occurs and already at about 80 K the peak intensities of the bands differ insignificantly. Beginning from $T \approx 100$ K the height of the band at 1.41 eV exceeds that corresponding to the band at 1.19 eV. At temperatures close to 300 K, the shape of the integral spectrum is practically determined by the first broad band E_{PL1}. The maximum of this band at room temperature is located at 1.4 eV. On excitation with the wavelength of $\lambda_{exR} = 633$ nm that falls within the E_{A1} broad absorption band (figure 1), the main contribution to the PL spectra in the whole temperature range is provided by the component at $E_{PL1} = 1.41$ eV (figure 3). It is worth noting that at room temperature the spectra obtained under 'red' and 'green' excitation have practically the same shape and peak position. It has to be mentioned that the intrinsic PL of the undoped samples [23], excited by the 248 nm (5 eV) line of a KrF excimer laser, has shown an ultraviolet spectral peak at 3.25 eV (296 K).

The time-resolved PL spectra measured under pulsed excitation with wavelengths: 'green'— $\lambda_{exGP} = 532$ nm are presented in figure 4. On 'green' pulsed excitation, three relatively sharp spectral lines located at $E_{PL3a} = 1.45$ eV, $E_{PL3b} = 1.49$ eV (E_{PL3b}–$E_{PL3a} = 39$ meV) and $E_{PL3c} = 1.505$ eV are revealed. These lines disappear in a very short time (less than ~ 1 μs) after the exciting pulse (time resolution ~ 0.1 μs) and can be observed only at low temperatures ($T < 90$ K). Under 'red' pulsed excitation $\lambda_{exRP} = 630$ nm (close to λ_{exR}) this sharp line emission does not arise. It should be noted that the E_{PL3} components can also be observed at low temperatures as a small feature on the short wavelength shoulder of the steady-state PL spectra obtained at 'green' excitation (figure 2, inset).

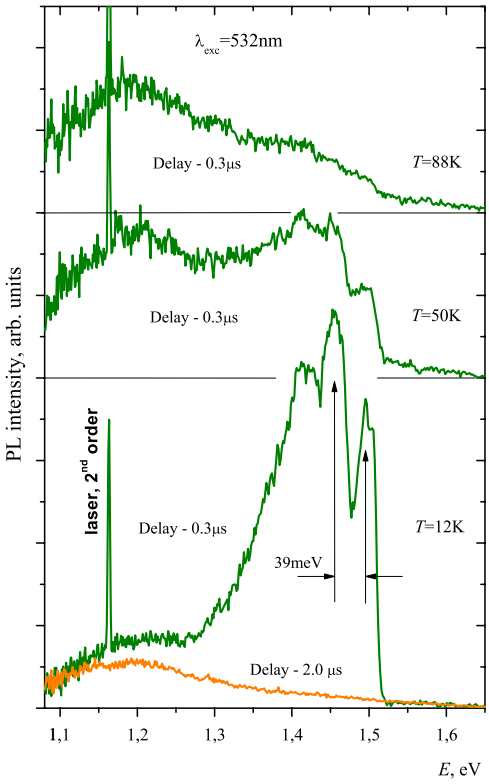

Figure 4. Time-resolved PL spectra under 'green' pulsed excitation.

3. Discussion

In order to explain the observed spectral transformations we employ the results of the EPR measurements which apparently show that the Ti impurity is EPR-silent in α-$ZnAl_2S_4$ crystals. This allows us to make up a conclusion that there is no Ti^{3+} and Ti^{2+} valence states. Otherwise, as in papers [16–19] dealing with impurity titanium ions in sulfur surroundings (see section 1), an EPR signal should be observed. Spectroscopic data on impurity CdS:Ti^{2+} and CdSe:Ti^{2+} systems [11, 14] show three absorption bands in the range of approximately 9000, 5000 and 3000 cm^{-1}. However, in the absorption spectra of the examined $ZnAl_2S_4$:Ti compound the bands are located at 19 360, 25 000 and 27 424 cm^{-1} (figure 1) and cannot be attributed to Ti^{2+} ions. In ZnS doped by Ti^{2+} ions [19], as was already mentioned above, the luminescence spectrum under excitation at 458 nm was observed in the range of 3600 cm^{-1}. A luminescence band centered at 4500 cm^{-1} corresponds to the $^2T_2 \rightarrow {}^2E$ emission of Ti^{3+} in ZnS [19] under the same excitation wavelength. However, the luminescence spectrum of titanium-doped α-$ZnAl_2S_4$ consists of two broad bands

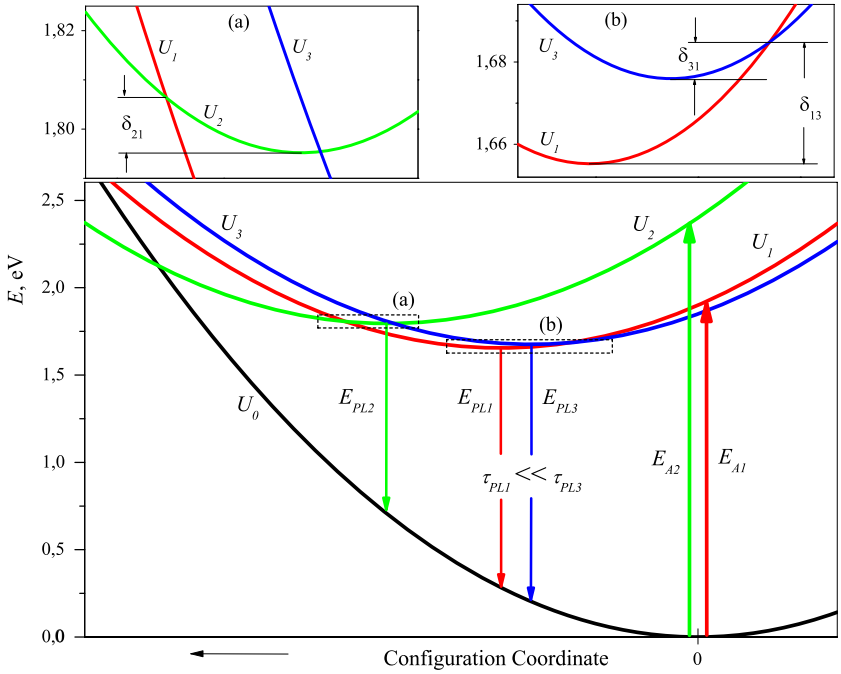

Figure 5. Single configuration-coordinate diagram for the TiS_6 complex in α-$ZnAl_2S_4$.

centered at $E_{PL1} = 1.41$ eV (11 373 cm^{-1}) and $E_{PL2} = 1.19$ eV (9600 cm^{-1}) and does not manifest similar features to those of Ti^{2+} and Ti^{3+} ions in ZnS [19]. Then, if the presence of Ti^{3+} and Ti^{2+} ions is not confirmed by EPR and optical spectra, it is logical to assume that titanium is present as Ti^{4+} (ionic radius 0.61 Å [24]) occupying the Al^{3+} site (ionic radius 0.67 Å [24]). Since the α-$ZnAl_2S_4$ semiconductor has a wide indirect bandgap ($E_g^{ind}(80\ K) = 3.50$ eV [11]) we assign the observed IR emission bands to the ligand-Ti^{4+} charge-transfer transitions. In favor of this assumption the following proof can also be adduced. The one-electron energies of the 3p sulfur and 3d titanium electrons in free atoms are equal to −0.86 and −0.68 Ryd [25], respectively. Thus, the energy of the electron transfer from the 3p orbital of sulfur to the 3d orbital of titanium is equal to 0.18 Ryd or 19 746 cm^{-1}. This value, which does not account for the crystal field splitting of the 3d state, is very close to the energy of the observed absorption band at 2.40 eV (19 360 cm^{-1}) in $ZnAl_2S_4$:Ti.

Therefore, further on we discuss the observed PL spectra in terms of a cluster composed of the central Ti^{4+} ion and six sulfur ligands. The ground state of this cluster is the $^1A_{1g}$ state. The configuration of this state can be illustratively written as $[Ti^{4+}(t_{2g}^0 e_g^0), {}^1A_{1g}]\,[S_6, {}^1A_{1g}]$. With the aid of the schematic MO energy-level diagram for an octahedrally coordinated Ti ion (TiL_6 cluster, where L is a ligand) presented in [26] it follows that the excited states of the TiS_6 complex characterized by odd parity arise from the electronic configurations $t_{2g}t_{1u}^5$ and $t_{2g}t_{2u}^5$ that contain an electron in the t_{2g} shell and a hole in the t_{1u} or t_{2u} shell. The configuration $t_{2g}t_{1u}^5$ gives rise to states with all possible combinations of $S = 0, 1$ and $\Gamma = A_{2u}, T_{1u}, T_{2u}, E_u$. For states arising from the configuration $t_{2g}t_{2u}^5$ $S = 0, 1$, while $\Gamma = A_{1u}, T_{1u}, T_{2u}, E_u$. The PL transitions $^{2S+1}A_{2u}, {}^{2S+1}A_{1u}, {}^{2S+1}T_{2u}, {}^{2S+1}E_u \rightarrow {}^1A_{1g}$ ($S = 0, 1$) are dipole-forbidden, while in the case of $\Delta S = 1$ some of these transitions are also spin-forbidden ($\Delta S = 1$). The allowed electric-dipole transitions are $^1T_{1u}^c \rightarrow {}^1A_{1g}$, where $c = a, b$, and $^1T_{1u}^a$ and $^1T_{1u}^b$ denote the lower and the higher in energy states arising from mixing of the $^1T_{1u}(t_{2g}t_{1u}^5)$ and $^1T_{1u}(t_{2g}t_{2u}^5)$ terms by the Coulomb interaction. At the same time according to Hund's rule the lowest in energy excited state is the $^3T_{1u}^a$ state. The labeling of this state has the same sense as in the case of the $^1T_{1u}^a$ state, with the only difference being that the two states $^3T_{1u}^c$ ($c = a, b$) arise from the mixing of the terms $^3T_{1u}(t_{2g}t_{1u}^5)$ and $^3T_{1u}(t_{2g}t_{2u}^5)$ by Coulomb interaction. The PL transition $^3T_{1u}^a \rightarrow {}^1A_{1g}$ is spin-forbidden but dipole-allowed. Basing on these considerations we assume that the two observed IR bands can be possibly assigned to the $^3T_{1u}^a \rightarrow {}^1A_{1g}$ and $^1T_{1u}^a \rightarrow {}^1A_{1g}$ transitions.

As was mentioned above the excitation by green light leads to the appearance of short-living narrow lines (figure 4) in the PL spectra at low temperatures. With a temperature rise these lines cannot be discerned; they merge with the broad band having the peak position at 1.1 μm. The origin of these lines may probably be assigned to spin-and dipole-forbidden transitions of the type of $^3E_u \rightarrow {}^1A_{1g}$ and $^3A_{1(2)u} \rightarrow {}^1A_{1g}$. These transitions represent an analog of the well-known optical transition $^2E_g \rightarrow {}^4A_{2g}$ in ruby and in α-$ZnAl_2S_4$:Cr [23] which manifests itself in the low-temperature PL spectra as a narrow zero-phonon R line that disappears at higher temperatures. As to the optical transitions facilitated by electron transfer between the orbitals t_{2g} and t_{1g} they are parity-forbidden and, therefore, are not included in this consideration.

The performed analysis of the experimental data allows us to assume that the energy spectrum of the TiS_6 complex can be conditionally illustrated by four adiabatic potential sheets (figure 5). The ground adiabatic potential sheet $^1A_{1g}$ looks as

follows:

$$U_0 = \frac{\hbar\omega}{2}q^2, \tag{1}$$

where $\hbar\omega$ is the energy of the vibrational quantum. The expressions for the first $^3T^a_{1u}$ and second $^1T^a_{1u}$ excited sheets:

$$U_1 = \frac{\hbar\omega}{2}q^2 + \Delta_1 + \upsilon_1 q, \qquad U_2 = \frac{\hbar\omega}{2}q^2 + \Delta_2 + \upsilon_2 q \tag{2}$$

include the energy gaps Δ_1 and Δ_2 between the ground $^1A_1$ and excited states (respectively, $^3T_1$ and $^1T_1$) in the rigid lattice, as well as the terms responsible for the interaction of the $^3T_1$ and $^1T_1$ states with the fully symmetric vibration of the TiS_6 complex. Finally, υ_1 and υ_2 are the corresponding vibronic coupling constants. In the adiabatic approximation the maxima of the luminescence bands under 'red' (E_{PL1}) and 'green' (E_{PL2}) excitation can be described by the following relations:

$$E_{PL1} = \Delta_1 - \upsilon_1^2/\hbar\omega, \qquad E_{PL2} = \Delta_2 - \upsilon_2^2/\hbar\omega. \tag{3}$$

Hereafter we assume that the gaps Δ_1 and Δ_2 are approximately equal to the energies of the A_1 and A_2 absorption bands $\Delta_1 = E_{A1} \approx 1.9$ eV and $\Delta_2 = E_{A2} \approx 2.4$ eV (figure 1). Taking into account the experimental values $E_{PL1} \approx 1.41$ eV, $E_{PL2} \approx 1.19$ eV and $\hbar\omega = 39$ meV $= 315$ cm^{-1} we obtain the vibronic coupling constants $\upsilon_1 = 138$ meV $= 1115$ cm^{-1} and $\upsilon_2 = 217$ meV $= 1753$ cm^{-1} and the height of the activation barrier:

$$\delta_{12} = \frac{\hbar\omega}{2}\left(\frac{\Delta_1 - \Delta_2}{\upsilon_2 - \upsilon_1} + \frac{\upsilon_2}{\hbar\omega}\right)^2 \simeq 11 \text{ meV}. \tag{4}$$

The estimated barrier height $\delta_{12} = 11$ meV $= 130$ K (figure 5(a)) is in good accordance with the experimental value $T \approx 120$ K at which the intensity of the luminescence band E_{PL1} becomes higher than that of the E_{PL2} band. Under 'green' excitation and $T \leqslant 80$ K, when only the minimum of the adiabatic potential sheet complying with the $^1T^a_{1u}$ state is populated, the maximum of the emission band corresponds to $E_{PL2} = 1.19$ eV. With a temperature rise the tunneling through the barrier δ_{21} leads to the population of the adiabatic potential sheet minimum related to the $^3T^a_{1u}$ state, and in the PL spectra, along with the band E_{PL2} the band E_{PL1} appears. At $T > 200$ K this band dominates in the spectra. Thus, at 'green' excitation significant changes in the shape of the luminescence band with temperature increase can be observed as a result of depopulation of the minimum of the adiabatic potential $U_{^1T_1}$ and simultaneous population of the minimum of the adiabatic potential sheet $U_{^3T_1}$ due to the tunneling through the barrier. Such a process can take place because the tunneling through the barrier in this case occurs much faster than the spontaneous decay of the $^1T_1$ state.

The probabilities of the radiative spin-and dipole-forbidden transitions of the type of $^3E_u \rightarrow {}^1A_{1g}$ and $^3A_{1(2)u} \rightarrow {}^1A_{1g}$ (figure 4) giving rise to short-living narrow lines (E_{PL3} component clearly seen at low temperatures) are small compared with that of the radiative $^3T^a_{1u} \rightarrow {}^1A_{1g}$ transition ($\tau_{PL1} \ll \tau_{PL3}$). Therefore, the disappearance of the fine structure of the band in the region of 1.3–1.55 eV in the time-resolved PL spectra (figure 4) at sufficiently low temperatures and, hence, the depopulation of the minima of the adiabatic potential sheets corresponding to the states ^3E_u and $^3A_{1(2)u}$ can be referred to the fast tunneling of the excitation through a comparatively low barrier separating these sheets and the $^3T^a_{1u}$ adiabatic potential sheet. The family of excited adiabatic potential sheets giving rise to the clearly distinguished lines in the low-temperature range will be substituted by one 'effective' adiabatic potential sheet described by the expression

$$U_3 = \frac{\hbar\omega}{2}q^2 + \Delta_3 + \upsilon_3 q \tag{5}$$

with the effective parameters Δ_3 and υ_3. The average position of the band corresponding to the transition from the minimum of the adiabatic potential sheet U_3 to the ground U_{A_1} sheet is determined as

$$E_{PL3} = \Delta_3 - \frac{\upsilon_3^2}{\hbar\omega}. \tag{6}$$

For E_{PL3} (figure 2) we approximately take the value $E_{PL3c} \approx 1.505$ eV. However, this experimental value is not enough for the determination from equation (6) of both the parameters Δ_3 and υ_3 characterizing the shape of the adiabatic potential U_3. Therefore, further for the estimation of these microscopic parameters we use the experimental value $\delta_{31} \approx 100$ K for the height of the barrier separating the sheets U_1 and U_3. This value corresponds to the temperature at which the fine structure of the spectrum in the energy range of 1.35–1.55 eV disappears. The analytical expression for δ_{13} looks as follows:

$$\delta_{31} = \frac{\hbar\omega}{2}\left(\frac{\Delta_3 - \Delta_1}{\upsilon_1 - \upsilon_3} + \frac{\upsilon_3}{\hbar\omega}\right)^2. \tag{7}$$

The solution of the system of equations (6) and (7) gives two sets of parameters Δ_3 and υ_3 close in magnitude: (1) $\Delta_3 = 1.85$ eV $\approx 14\,920$ cm^{-1} and $\upsilon_3 = 116$ meV ≈ 940 cm^{-1}; (2) $\Delta_3 = 1.79$ eV $\approx 14\,440$ cm^{-1} and $\upsilon_3 = 105$ meV ≈ 850 cm^{-1}. However, only the first set corresponds to the configuration that is in accordance with the experimental data. Indeed, in this case the U_3 potential's minimum is located above the minimum of the potential U_1 ($\delta_{13} > \delta_{31}$, figure 5(b)) and, taking into account the inequality $\tau_{PL1} \ll \tau_{PL3}$, it is obvious that in such a configuration the E_{PL3} emission component (transitions $^3E_u \rightarrow {}^1A_{1g}$ or $^3A_{1(2)u} \rightarrow {}^1A_{1g}$) can be excited only via the potential U_2 ($^1T^a_{1u}$ state) using the 'green' radiation—the excitation by 'red' radiation is excluded. The second set of parameters Δ_3 and υ_3 corresponds to the inverse reciprocal location of U_1 and U_3 minima ($\delta_{31} > \delta_{13}$) and gives the possibility to excite the E_{PL3} component through potential U_1 ($^3T^a_{1u}$ state), i.e. using the 'red' pumping that experimentally was not observed.

Thus the picture of the adiabatic potential sheets represented in figure 5 gives a clear qualitative explanation of the observed spectroscopic data.

4. Concluding remarks

The luminescent properties of the α-$ZnAl_2S_4$:Ti system and the kinetics of luminescence decay have been examined.

On the basis of combined optical and EPR studies the observed PL spectra are assigned to ligand-Ti^{4+} charge-transfer transitions in a complex consisting of a Ti^{4+} ion and six sulfur atoms. An energy diagram is suggested to explain the temperature behavior of the observed PL spectra under different wavelengths of optical excitation. With the aid of experimental data the microscopic parameters characterizing the states of the TiS_6 complex involved in optical transitions in the range of 0.8–1.7 eV are determined.

In our further work we are going to support the qualitative explanation of the experimental data with quantum-mechanical calculations of the energies of electron transitions and probabilities of intracenter nonradiative transitions. The calculation of the shapes of the absorption and PL bands on the basis of the solution of the vibronic dynamic problems for the excited $^1T^a_{1u}$ and $^3T^a_{1u}$ states will also be undertaken.

References

[1] Moulton P 1982 *Opt. Photon. News* **8** 9
[2] Schepler K L and Kokta M 1988 *J. Appl. Phys.* **63** 960
[3] Kodama N and Yamaga M 1998 *Phys. Rev.* B **57** 811
[4] Bausa L E, Vergara I, Garcia-Solé J, Strek W and Deren P J 1990 *J. Appl. Phys.* **68** 736
[5] Jouini A, Yoshikawa A, Brenier A, Fukuda T and Boulon G 2007 *Phys. Status Solidi* c **4** 1380
[6] Yamaga M, Yosida T, Hara S, Kodama N and Henderson B 1994 *J. Appl. Phys.* **75** 1111
[7] Wegner T and Petermann K 1989 *Appl. Phys.* B **49** 275
[8] Wong W C, McClure D S, Basun S A and Kokta M R 1995 *Phys. Rev.* B **51** 5682
Wong W C, McClure D S, Basun S A and Kokta M R 1995 *Phys. Rev.* B **51** 5693
[9] Sato T, Shirai M, Tanake K, Kawabe K and Hanamura E 2005 *J. Lumin.* **114** 155
[10] Boyn R, Dziesiaty J and Wruck D 1970 *Phys. Status Solidi* **42** K197
[11] Boyn R and Ruszczynski G 1971 *Phys. Status Solidi* b **48** 643
[12] Rosenfeld A, Boyn R and Ruszczynski G 1975 *Phys. Status Solidi* b **70** 601
[13] Ruszczynski G and Boyn R 1976 *Phys. Status Solidi* b **76** 427
[14] Langer J M and Baranowski J M 1971 *Phys. Status Solidi* b **44** 155
[15] Kosot K and Baranowski J M 1977 *Phys. Status Solidi* b **81** 629
[16] Böttcher R and Dziesiaty J 1972 *Phys. Status Solidi* b **53** 505
[17] Böttcher R and Dziesiaty J 1973 *Phys. Status Solidi* b **57** 617
[18] Peka P, Lehr MU, Schulz H-J, Dziesiaty J and Müller S 1996 *J. Cryst. Growth* **161** 277
[19] Dziesiaty J, Lehr M U, Peka P, Klimakov A, Müller S and Schulz H J 1998 *Eur. Phys. J.* B **4** 269
[20] Berthold H J and Köhler K 1981 *Z. Anorg. Allg. Chem.* **475** 45
[21] Kulikova O V, Moldovyan N A, Popov S M, Radautsan S I and Siminel A V 1993 *Japan. J. Appl. Phys* **32** (Suppl. 32-3) 586
[22] Kai T, Kaifuku M, Aksenov I and Sato K 1995 *Japan. J. Appl. Phys.* **34** 3073
[23] Broussell I, Fortin E, Kulyuk L, Popov S, Anedda A and Corpino R 1998 *J. Appl. Phys.* **84** 533
[24] Shannon R D 1976 *Acta Crystallogr.* A **32** 751
[25] Slater J C 1955 *Phys. Rev.* **98** 1039
[26] Ballhausen C J and Gray H B 1964 *Molecular Orbital Theory* (London: Benjamin/Cummings) p 103